

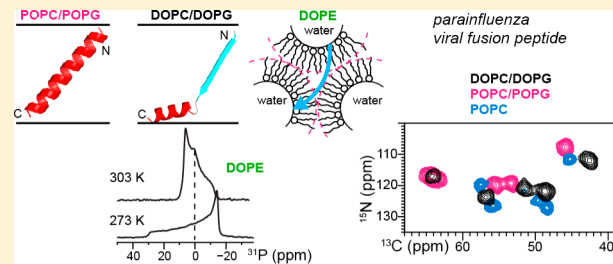
# Conformation and Lipid Interaction of the Fusion Peptide of the Paramyxovirus PIV5 in Anionic and Negative-Curvature Membranes from Solid-State NMR

Hongwei Yao and Mei Hong\*

Department of Chemistry, Iowa State University, Ames, Iowa 50011 United States

## Supporting Information

**ABSTRACT:** Viral fusion proteins catalyze the merger of the virus envelope and the target cell membrane through multiple steps of protein conformational changes. The fusion peptide domain of these proteins is important for membrane fusion, but how it causes membrane curvature and dehydration is still poorly understood. We now use solid-state NMR spectroscopy to investigate the conformation, topology, and lipid and water interactions of the fusion peptide of the PIV5 virus F protein in three lipid membranes, POPC/POPG, DOPC/DOPG, and DOPE. These membranes allow us to investigate the effects of lipid chain disorder, membrane surface charge, and intrinsic negative curvature on the fusion peptide structure. Chemical shifts and spin diffusion data indicate that the PIV5 fusion peptide is inserted into all three membranes but adopts distinct conformations: it is fully  $\alpha$ -helical in the POPC/POPG membrane, adopts a mixed strand/helix conformation in the DOPC/DOPG membrane, and is primarily a  $\beta$ -strand in the DOPE membrane.  $^{31}\text{P}$  NMR spectra show that the peptide retains the lamellar structure and hydration of the two anionic membranes. However, it dehydrates the DOPE membrane, destabilizes its inverted hexagonal phase, and creates an isotropic phase that is most likely a cubic phase. The ability of the  $\beta$ -strand conformation of the fusion peptide to generate negative Gaussian curvature and to dehydrate the membrane may be important for the formation of hemifusion intermediates in the membrane fusion pathway.



## INTRODUCTION

The parainfluenza virus 5 (PIV5) belongs to the *paramyxoviridae* family, which contains significant pathogens to mammals such as measles, mumps, and Hendra viruses.<sup>1–3</sup> These enveloped viruses enter cells through virus–cell membrane fusion. Two glycoproteins in the lipid envelope, a receptor-binding protein (HN, H, or G) and a fusion protein (F), are required for membrane fusion.<sup>4,5</sup> The F protein, similar to the influenza hemagglutinin (HA) and the HIV Env protein, is synthesized as a homotrimer and is activated by proteolytic cleavage, which creates a highly hydrophobic N terminus called the fusion peptide (FP) that is essential for membrane fusion.<sup>6,7</sup> The cleaved protein is anchored to the virus envelope by a hydrophobic C-terminal transmembrane (TM) domain.<sup>8</sup> Two heptad repeats, HRA and HRB, lie next to the FP and TM domains, respectively.

Crystal structures of the water-soluble portions of a number of viral fusion proteins<sup>9–11</sup> have been determined and have provided much of the current understanding of the mechanism of protein-mediated virus–cell membrane fusion. It is known that fusion proteins undergo multiple conformational changes to provide the necessary energy for membrane fusion.<sup>12,13</sup> The conformations that have been observed correspond to the prefusion states before and after cleavage, an extended prehairpin state and the postfusion hairpin state. The hairpins are formed between two heptad-repeat domains common in class I fusion proteins and give rise to a six-helix bundle (6HB) that is

characteristic of the postfusion state of these trimeric proteins.<sup>14–20</sup> A consequence of this 6HB is that it enforces close proximity of the neighboring FP and TM domains in the merged membrane, but no direct structural evidence of this close packing in the membrane has yet been reported. For the parainfluenza F protein, the crystal structures of the uncleaved prefusion state,<sup>21</sup> the cleaved prefusion state,<sup>22</sup> and the postfusion state<sup>19</sup> have been determined, and an extended prehairpin structure was observed by electron microscopy.<sup>23</sup> In comparison, structural information about the membrane-bound FP and TM domains is still scarce.

Solution and solid-state NMR studies of the influenza and HIV fusion peptides in detergent micelles and lipid bilayers have provided insights into the mechanisms of virus–cell fusion.<sup>24–30</sup> The HA fusion peptide is predominantly  $\alpha$ -helical, but the exact tertiary structure depends on the peptide length and the membrane-mimetic environment. A 20-residue construct adopts an obliquely inserted boomerang conformation in detergent micelles,<sup>24,31–34</sup> but in lipid bilayers at fusogenic pH, it also samples a small population of a helical hairpin conformation.<sup>35</sup> A 23-residue construct that includes the conserved GxxxG and GxxG motifs adopts a helical hairpin conformation already in detergent micelles, with the hairpin stabilized by Gly–Gly interactions at the helix interface.<sup>29</sup> Gly to Ala mutation at

Received: November 29, 2013

Published: January 16, 2014

**Table 1.**  $^{13}\text{C}$ - $^{15}\text{N}$ -Labeled FPK4 Peptides Used in This Work<sup>a</sup>

sample	labeled residue
GVAL	G114, V115, A126, L127
IGALV	I108, G109, A112, L113, V125
GVTAA	G105, V106, T122, A123, A124
VLAAT	V107, L110, A111, A116, T117
AAQV	A118, A119, Q120, V121

<sup>a</sup>FPK4(103–129): FAGVVIGLAALGVATAAQVTAVALVK-DIOXA-KKKK.

residue 8 results in a mixture of hairpin and boomerang structures.<sup>30,36</sup> The HIV fusion peptide has a more complex conformational behavior. It is  $\alpha$ -helical in detergent micelles<sup>25,28,37</sup> but a  $\beta$ -strand in lipid bilayers containing more than ~20% cholesterol.<sup>38–40</sup> Temperature and peptide concentration also affect the HIV fusion peptide structure.<sup>41–43</sup> Solid-state NMR data indicate that both helical and strand conformations of the HIV FP insert into the lipid membrane but cross-linked trimers insert more deeply than monomers and are also more fusogenic.<sup>44</sup>

The conformational polymorphism of these viral fusion peptides indicates the importance of the lipid environment in regulating membrane fusion.<sup>45</sup> However, the lipid environment is important not only for modulating the FP structure but also for directly influencing the membrane curvature and hydration during fusion. A large number of computational analyses<sup>46–48</sup> and experimental studies have probed the structures of membrane intermediates during fusion;<sup>49–51</sup> however, few studies have combined or correlated the FP structure with the membrane-intermediate structure.

We recently reported the first solid-state NMR structural study of the PIVS fusion peptide in lipid bilayers.<sup>52</sup> We found that the peptide adopted an  $\alpha$ -helical conformation in the negatively charged POPC/POPG membrane but a  $\beta$ -strand conformation on the surface of neutral POPC and DMPC bilayers. In the current study, we have determined the complete backbone conformation of the POPC/POPG-bound PIVS FP using chemical shift constraints. We further extend the structural study to two other lipid membranes. The DOPC/DOPG membrane retains the same negative surface charge as the POPC/POPG membrane but increases the unsaturation and disorder of the lipid

chains. Surprisingly, this change did not increase the FP mobility but converted the peptide from an  $\alpha$ -helical structure to a partial  $\beta$ -strand structure. In the DOPE membrane, the PIVS fusion peptide mainly adopts a  $\beta$ -strand conformation, similar to its structure in neutral PC membranes, but the  $\beta$ -strand is inserted into the DOPE membrane rather than surface bound. Moreover, the peptide changes the phase behavior and hydration of the DOPE membrane. These results suggest the structural roles of the PIVS fusion peptide during membrane fusion.

## EXPERIMENTAL SECTION

**Peptide and Lipids.** The fusion peptide used in this study corresponds to residues 103–129 of the PIVS F protein, with the amino acid sequence of FAGVVIGLAALGVATAAQVTAVALVK. To increase the peptide solubility, a Lys tag KKKK was appended to the C terminus through a flexible DIOXA linker ( $-\text{NH}(\text{CH}_2\text{CH}_2\text{O})_2\text{CH}_2\text{CO}-$ ). This construct is called FPK4 in this work. Five  $^{13}\text{C}$ - $^{15}\text{N}$ -labeled peptides were synthesized by Primm Biotech (Cambridge, MA): GVAL-FPK4, IGALV-FPK4, GVTAA-FPK4, VLAAT-FPK4, and AAQV-FPK4 (Table 1). The labeled residues cover all except for four residues at the N and C termini (F103, A104, V128, and K129) of the peptide.

FPK4 was reconstituted into POPC/POPG (4:1), DOPC/DOPG (4:1), and DOPE membranes at a peptide/lipid molar ratio of 1:20. The samples were prepared as previously described.<sup>52</sup> Briefly, the peptide was dissolved in trifluoroethanol (TFE) and mixed with lipids in chloroform. The solvent was removed under nitrogen gas, and the sample was lyophilized. The homogeneous powder was suspended either in Tris buffer (10 mM Tris-HCl, 1 mM EDTA, 1 mM Na<sub>3</sub>N, pH 7.5) or phosphate buffer (10 mM Na<sub>2</sub>HPO<sub>4</sub>-NaH<sub>2</sub>PO<sub>4</sub>, 1 mM EDTA, 1 mM Na<sub>3</sub>N, pH 7.5) and dialyzed for a day. The proteoliposomes were centrifuged at 55 000 rpm at 4 °C to obtain membrane pellets, which were equilibrated to 30–40 wt % water before being transferred to 4 mm magic-angle-spinning (MAS) rotors.

**Solid-State NMR Experiments.** MAS NMR experiments were carried out on Bruker AVANCE-600 (14.1 T) and DSX-400 MHz (9.4 T) spectrometers.  $^{13}\text{C}$  chemical shifts were referenced to the adamantane CH<sub>2</sub> signal at 38.48 ppm on the TMS scale, and the  $^{15}\text{N}$  chemical shifts were referenced to the N-acetylvaline signal at 122.0 ppm on the liquid ammonia scale.  $^{31}\text{P}$  chemical shifts were referenced to the hydroxypapatite signal at 2.73 ppm on the phosphoric acid scale.

Two-dimensional (2D)  $^{13}\text{C}$ - $^{13}\text{C}$  correlation spectra were measured using a  $^1\text{H}$ -driven  $^{13}\text{C}$  spin diffusion experiment with  $^1\text{H}$  irradiation (DARR)<sup>53</sup> during a mixing time of 20–60 ms. Experimental temperatures ranged from 233 to 303 K to investigate FPK4 conformation in both the gel and liquid-crystalline (LC) phases of the membrane. 2D  $^{15}\text{N}$ - $^{13}\text{C}$  correlation spectra were measured using a REDOR-based pulse sequence<sup>54</sup> with a coherence transfer time of 857  $\mu$ s. 2D spectra

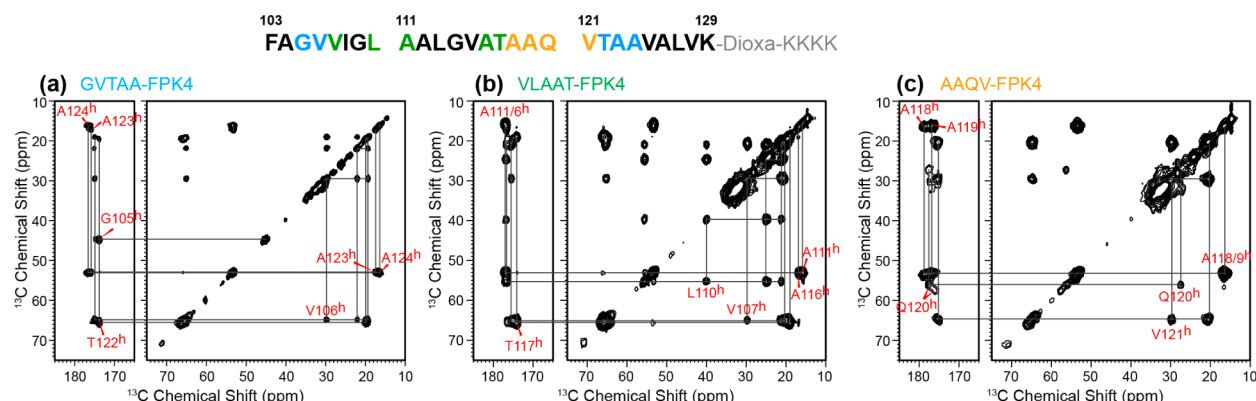


**Figure 1.** 2D  $^{13}\text{C}$ - $^{13}\text{C}$  correlation spectra of PIVS FPK4 in gel-phase POPC/POPG (4:1) bilayers. Shown at the top is the amino acid sequence with labeled residues color-coded according to samples. (a) GVTAA-FPK4 spectrum, measured at 253 K with 20 ms mixing. (b) VLAAT-FPK4 spectrum, coadded from two spectra measured at 243 K with 20 ms mixing and 253 K with 60 ms mixing. (c) AAQV-FPK4 spectrum, measured at 253 K with 20 ms mixing. All residues show resolved and  $\alpha$ -helical chemical shifts. Superscript h denotes helical chemical shifts.

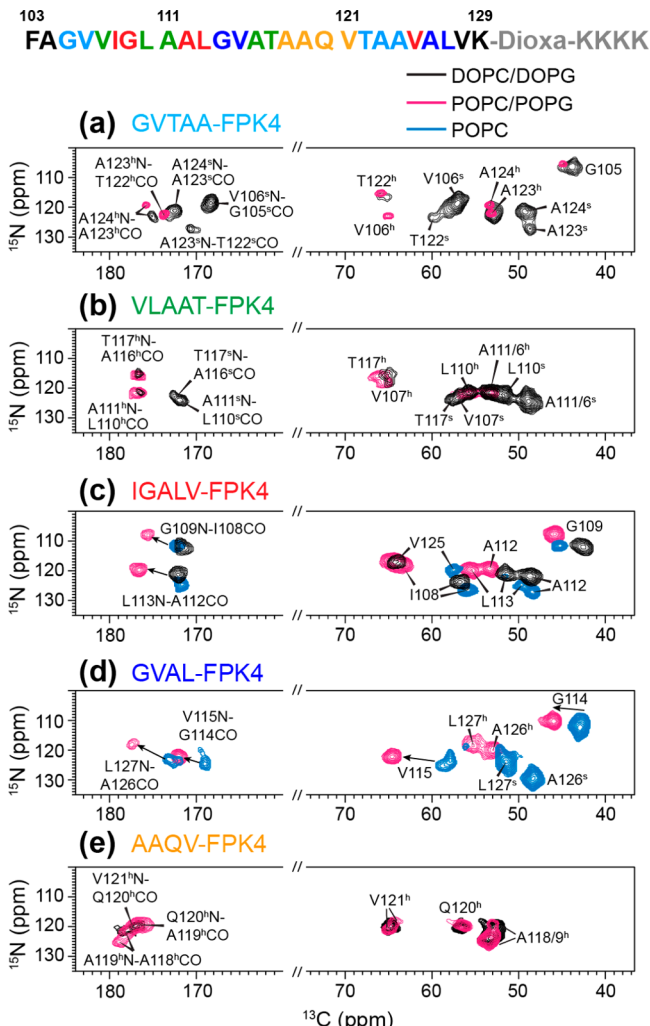


**Figure 2.** 2D  $^{15}\text{N}$ – $^{13}\text{C}$  correlation spectra of PIVS FPK4 in gel-phase POPC/POPG (magenta), DOPC/DOPG (black), and POPC (blue) membranes. (a) GVTAA-FPK4 spectra. (b) VLAAT-FPK4 spectra. (c) IGALV-FPK4 spectra. (d) GVAL-FPK4 spectra. (e) AAQV-FPK4 spectra. The peptide shows predominantly  $\beta$ -strand chemical shifts in the POPC membrane,  $\alpha$ -helical chemical shifts in the POPC/POPG membrane, and mixed strand and helix chemical shifts in the DOPC/DOPG membrane. Most residues in the GVTAA and VLAAT samples show two sets of chemical shifts in the DOPC/DOPG bilayer. The AAQV sample shows nearly identical  $\alpha$ -helical chemical shifts in the POPC/POPG and DOPC/DOPG membranes. Superscripts h and s denote helical and strand chemical shifts, respectively.

were measured under 7, 8, or 10.5 kHz spinning. One-dimensional (1D) static and MAS  $^{31}\text{P}$  spectra were measured between 273 and 313 K to probe the membrane morphology and structure. The size of the  $^{31}\text{P}$  chemical shift anisotropy (CSA) is characterized by its span, defined as the difference between the  $0^\circ$  edge and the  $90^\circ$  edge of the uniaxial powder pattern,  $\Delta\sigma = \sigma_{0^\circ} - \sigma_{90^\circ}$ . A 2D  $^{31}\text{P}$ – $^1\text{H}$  correlation experiment was conducted to measure the hydration of the lipid headgroups.<sup>52</sup>

The depth of insertion of the fusion peptide was measured using 2D  $^1\text{H}$  spin diffusion experiments in either the LC phase<sup>55,56</sup> or the gel phase.<sup>57</sup> The LC-phase experiment was applied to DOPC/DOPG-bound peptide with IGALV and AAQV labels using a  $^1\text{H}$   $T_2$  filter of 0.8–1.0 ms and a spin diffusion mixing time of 9–625 ms. Spin diffusion buildup curves were quantified after correcting for  $^1\text{H}$   $T_1$  relaxation and were simulated using diffusion coefficients of 0.012 and 0.30 nm $^2$ /ms for the lipid and peptide, respectively. The water–peptide interfacial diffusion coefficient ( $D_{WP}$ ) was 0.002–0.003 nm $^2$ /ms while the lipid–peptide coefficient ( $D_{LP}$ ) was 0.0025–0.005 nm $^2$ /ms. The gel-phase

spin diffusion experiment was carried out on POPC/POPG- and DOPC/DOPG-bound FPK4. The intensity ratios between the water and lipid  $\text{CH}_2$  cross peaks of each residue were measured to compare residue-specific depths.

## RESULTS

**Complete Backbone Conformation of FPK4 in the POPC/POPG Membrane.** We recently reported that POPC/POPG-bound FPK4 exhibited only  $\alpha$ -helical chemical shifts for nine labeled residues,<sup>52</sup> suggesting that this membrane promotes a single conformation of the peptide. To obtain the complete backbone conformation in this anionic membrane, we labeled additional residues (Table 1). Figures 1 and 2 show the 2D  $^{13}\text{C}$ – $^{13}\text{C}$  and  $^{15}\text{N}$ – $^{13}\text{C}$  correlation spectra of FPK4 in gel-phase POPC/POPG bilayers. Consistent with the previous study, most residues exhibited  $\alpha$ -helical chemical shifts and a single set of signals. Modest conformational disorder was manifested at residues A118–V121 as reduced intensities and peak multiplicity. For example, the Q120  $\text{Ca}$ – $\text{C}\beta$  cross peak is 4-fold weaker than the A118 and A119 peak (Figure 1c), suggesting dynamic disorder at Q120. These four residues also exhibit two sets of signals in the 2D  $^{15}\text{N}$ – $^{13}\text{C}$  spectra (Figure 2e), indicating static conformational disorder. A recent hexamer model of PIVS fusion peptide placed Q120 in the interior of the hexamer and postulated that this residue may be involved in intermolecular H-bonding.<sup>58</sup> Since oligomeric assembly and H-bonding should order and immobilize the peptide, our data does not support this model for FPK4 in the POPC/POPG membrane.

The assigned  $^{13}\text{C}$  and  $^{15}\text{N}$  chemical shifts of POPC/POPG-bound FPK4 (Table 2) allow us to obtain a backbone conformational model of the peptide. All 23 residues (G105–L127) exhibit  $\alpha$ -helical chemical shifts as the dominant signals, with positive  $\text{C}\alpha$  and  $\text{CO}$  secondary shifts and negative  $\text{C}\beta$  secondary shifts (Figure 3a). Using TALOS+,<sup>59</sup> we obtained backbone ( $\phi$ ,  $\psi$ ) torsion angles (Table 3), which indicate a nearly ideal  $\alpha$ -helical conformation in the POPC/POPG membrane.

**Depth of Insertion of FPK4 in the POPC/POPG Membrane.** FPK4 undergoes intermediate-time scale motion in the LC phase of the POPC/POPG membrane. The resulting line broadening precludes the LC-phase  $^1\text{H}$  spin diffusion experiment<sup>60</sup> for measuring the insertion depth of the peptide. Therefore, we carried out the gel-phase spin diffusion experiment,<sup>57</sup> which resolves the water, lipid, and peptide  $^1\text{H}$  signals in the indirect dimension by  $^1\text{H}$  homonuclear decoupling. Strong cross peaks between lipid protons and peptide  $^{13}\text{C}$  signals indicate deep insertion of the peptide into the membrane. In addition, well-inserted peptides exhibit similar  $^1\text{H}$  intensity patterns as the lipid chain carbons, while surface-bound peptides exhibit different  $^1\text{H}$  cross sections, with much higher water cross peaks than lipid cross peaks.

Figure 4a shows representative gel-phase  $^1\text{H}$  spin diffusion spectra of FPK4 in the POPC/POPG membrane. By 25 ms, the peptide shows strong cross peaks with both lipids and water, and the peptide  $\text{C}\alpha$  and lipid  $\text{CH}_2$  cross sections have similar  $^1\text{H}$  chemical shifts, linewidths, and intensity distributions (Figure 4b), indicating that FPK4 is well inserted into the hydrophobic region of the membrane. With a shorter mixing time of 4 ms, more residue-specific depth information is obtained, since different residues give different relative intensities between the water and lipid cross peaks (Figure 4c); terminal residues such as G105 and A126 have higher water/lipid intensity ratios than middle residues such as A112 and L113, indicating that the two termini are in closer contact with water. The water/lipid intensity

Table 2.  $^{13}\text{C}$  and  $^{15}\text{N}$  Chemical Shifts of PIVS FPK4 in POPC/POPG and DOPC/DOPG Membranes<sup>a</sup>

residue	POPC/POPG (4:1)						DOPC/DOPG (4:1)					
	N	CO	C $\alpha$	C $\beta$	C $\gamma$	C $\delta$	N	CO	C $\alpha$	C $\beta$	C $\gamma$	C $\delta$
G105 <sup>b</sup>	105.2	173.7	44.8				106.6	168.4	43.7			
V106 <sup>b</sup>	122.8	174.8	64.9	29.6	21.9/19.1		118.6	170.0	56.8	34.0	19.5/18.4	
V107 <sup>c</sup>	118.2	175.2	64.9	29.6	20.2		123.4	171.8	57.2	32.8	19.4	
							117.4	175.1	64.8	29.3	20.8/19.6	
I108 <sup>d</sup>	117.7	175.6	63.3	36.3	28.6/15.4	13.0	123.8	171.6	56.3	40.0	26.4/15.2	12.6
G109 <sup>d</sup>	107.7	173.6	45.5				112.1	168.3	42.3			
L110 <sup>c</sup>	121.8	176.6	55.3	39.8	24.7		122.3	171.8	51.3	44.7	24.6	
							121.4	176.7	55.5	39.5	24.6	20.7
A111 <sup>c</sup>	121.4	177.0	53.1	15.5			124.1	172.5	48.6	20.8		
							121.4	176.9	53.0	15.9		
A112 <sup>d</sup>	119.3	176.6	53.1	16.4			121.9	172.1	48.3	21.7		
							176.5	53.2	15.6			
L113 <sup>d</sup>	119.9	177.9	55.2	39.8	24.7	20.0	121.1	172.2	51.1	44.5	25.0	22.0
							178.2	55.2	39.3	24.6		
G114 <sup>e</sup>	110.4	171.9	45.7				ND					
V115 <sup>e</sup>	122.4	175.2	64.4	29.3	20.6/19.2		ND					
A116 <sup>c</sup>	121.4	176.7	53.1	16.6			121.5	176.9	53.0	15.9		
							124.5	172.5	48.6	20.8		
T117 <sup>c</sup>	115.8	173.8	65.5	65.5	18.8		115.1	173.7	65.2	65.2	19.2	
							123.8	173.3	57.6	68.5	20.0	
A118 <sup>f</sup>	124.6	178.6	53.3	16.2			123.6	178.6	52.8	16.0		
							173.1	48.7	21.0			
A119 <sup>f</sup>	124.6	176.6	53.3	16.3			120.4	176.6	52.8	16.0		
							173.1	48.7	21.0			
Q120 <sup>f</sup>	119.6	177.5	56.1	27.2	32.0		120.4	176.8	56.4	25.7	31.9	
V121 <sup>f</sup>	120.8	175.1	64.7	29.5	20.2		119.9	175.3	64.7	29.2	19.9	
								57.8		19.5		
T122 <sup>b</sup>	115.2	173.6	65.9	65.9	19.7		116.4	174.0	65.7	65.7	20.0	
							123.2	170.5	59.3	69.2	19.9	
A123 <sup>b</sup>	121.9	175.8	53.1	17.3			122.6	177.0	52.7	16.3		
							121.4	172.6	48.8	21.6		
A124 <sup>b</sup>	119.1	176.5	53.2	16.2			122.6	177.0	52.7	16.3		
							121.4	172.6	48.8	21.6		
V125 <sup>d</sup>	116.7	175.3	64.1	29.1	20.6		117.1	175.4	64.1	29.2	21.0/19.8	
A126 <sup>e</sup>	120.0	177.3	52.6	15.9			ND					
L127 <sup>e</sup>	118.6	175.7	55.0	40.0	24.8	21.5	ND					

<sup>a</sup>Chemical shifts were measured from 2D spectra at 233–253 K. Italics indicate the second conformation. <sup>13</sup>C chemical shifts are referenced to TMS, and <sup>15</sup>N chemical shifts are referenced to liquid ammonia. <sup>b</sup>From the GVTA sample (G105, V106, T122, A123, and A124). <sup>c</sup>From the VLAAT sample (V107, L110, A111, A116, and T117). <sup>d</sup>From the IGALV sample (I108, G109, A112, L113, and V125). <sup>e</sup>From the GVAL sample (G114, V115, A126, and L127). <sup>f</sup>From the AAQV sample (A118, A119, Q120, and V121).

ratios (Figure 4d) are the lowest between A111 and T117 (0.10–0.13) and higher for both the N and C termini (0.17–0.35), consistent with a membrane-spanning topology of the peptide. The intensity profile is asymmetric, with the N terminus having higher values than the C terminus, indicating that the N-terminal half of the peptide is more exposed to the membrane surface.

**FPK4 Has a Mixed Strand/Helix Conformation in the DOPC/DOPG Membrane.** Since FPK4 undergoes intermediate-time scale motion in the POPC/POPG membrane at ambient temperature, we searched for a different lipid membrane that may speed up the helix motion. Fast motion not only gives higher-resolution NMR spectra but may also allow helix orientation to be determined from motional order parameters without requiring macroscopically aligned samples.<sup>61,62</sup> The most obvious choice is the DOPC/DOPG (4:1) membrane, since it has the same membrane surface charge as the POPC/POPG bilayer while having a 18 °C lower gel-to-LC phase-transition temperature due to the presence of a double bond in both acyl chains of each lipid.

Surprisingly, the increased disorder and dynamics of the DOPC/DOPG membrane did not speed up motion of the fusion peptide but changed the peptide conformation. 1D <sup>13</sup>C CP-MAS spectra (Figure 5) show high-intensity  $\beta$ -strand signals for various residues at ambient temperature and few  $\alpha$ -helical signals. When the membrane is cooled to the gel phase, the  $\alpha$ -helix signals become detectable and comparable in intensity as the  $\beta$ -strand signals. Thus, the remaining  $\alpha$ -helical conformation has similar intermediate-time scale motion between the DOPC/DOPG and the POPC/POPG membranes, but the new  $\beta$ -strand structure is immobilized in the LC phase. The increased disorder of the lipid chains shifted the conformational equilibrium of the fusion peptide toward  $\beta$ -strand, without changing the mobility of the  $\alpha$ -helical segment.

Figure 6 shows 2D <sup>13</sup>C–<sup>13</sup>C DARR spectra of four labeled peptides in the gel and LC phases of the DOPC/DOPG membrane. In the gel phase, most residues show two sets of chemical shifts. The exceptions are G105, V106, I108, and G109, which

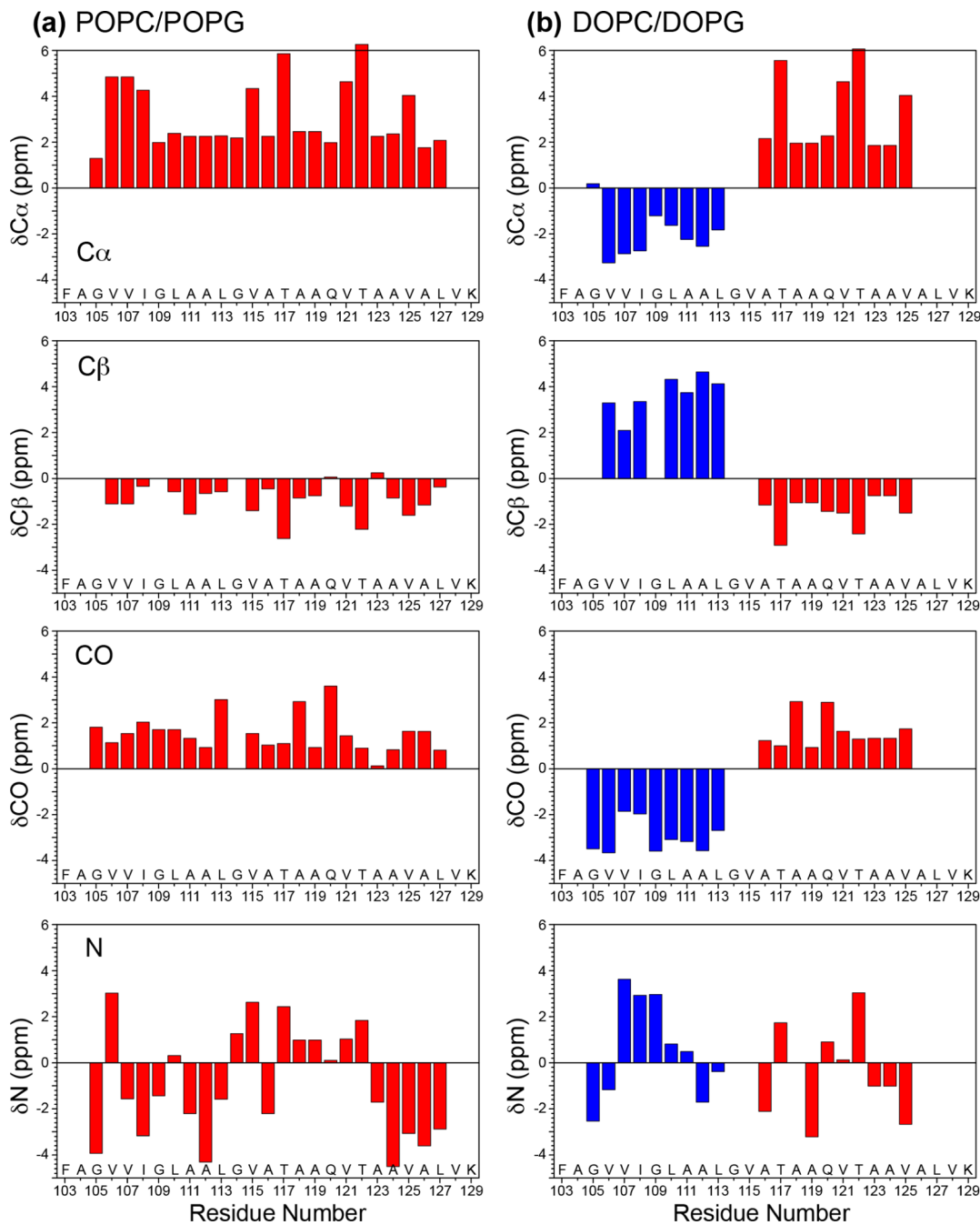


**Figure 3.**  $^{13}\text{C}$  and  $^{15}\text{N}$  secondary chemical shifts of FPK4 in (a) POPC/POPG and (b) DOPC/DOPG membranes. FPK4 shows clear  $\alpha$ -helical chemical shifts (red) in POPC/POPG bilayers and mixed helical and strand chemical shifts (blue) in DOPC/DOPG bilayers. The random coil values of Zhang et al.<sup>86</sup> were used to calculate the secondary shifts.

exhibit only  $\beta$ -strand signals, and Q120 and V125, which display only  $\alpha$ -helical chemical shifts. Increasing the temperature decreased the intensities of the helix signals while retaining the strand signals. The position of the peptide at which the helix and strand have comparable intensities is T117. The signals of several Ala residues partially overlap in the short-mixing-time spectra but become resolved by inter-residue cross peaks at long mixing times. For example, the 300 ms 2D spectrum (Figure S1a, Supporting Information) shows  $\beta$ -strand L110–A111 cross peaks and  $\alpha$ -helical A116–T117 cross peaks, indicating that A111 is primarily in the strand conformation while A116 is mostly helical. A118 and A119 show chemical shifts for all three conformations, but the  $\alpha$ -helix intensity dominates the strand

and coil intensities (Figure 6g, h). Finally, the N-terminal half of the peptide underwent a slow conformational change from  $\alpha$ -helical to  $\beta$ -strand in the DOPC/DOPG membrane: V107, L110, and A111 initially showed  $\alpha$ -helical chemical shifts, which converted to  $\beta$ -strand chemical shifts at equilibrium (Figure S1b, Supporting Information). However, the more C-terminal A116 and T117 in the same VLAAT sample remained stably  $\alpha$ -helical.

2D  $^{15}\text{N}$ – $^{13}\text{C}$  correlation spectra (Figure 2) confirmed the mixed strand/helix conformation of the N- and C-terminal halves of the DOPC/DOPG-bound peptide. Two sets of chemical shifts were observed for many residues, but residues G105–L113 show dominant  $\beta$ -strand peaks while residues A118–V125 have dominant  $\alpha$ -helical peaks. Comparison of the peptide spectra for

**Table 3. Backbone ( $\varphi$ ,  $\psi$ ) Torsion Angles of PIV5 FPK4 in POPC/POPG and DOPC/DOPG Membranes Predicted Using TALOS+<sup>a</sup>**

residue	POPC/POPG (4:1)		DOPC/DOPG (4:1)	
	$\varphi$ (deg)	$\psi$ (deg)	$\varphi$ (deg)	$\psi$ (deg)
V106	-65 ± 4	-44 ± 5	-135 ± 19	146 ± 17
V107	-61 ± 6	-41 ± 10	-124 ± 11	140 ± 17
I108	-64 ± 10	-38 ± 16	-130 ± 13	143 ± 15
G109	-63 ± 5	-39 ± 4	-142 ± 19	156 ± 18
L110	-64 ± 4	-42 ± 7	-136 ± 11	146 ± 12
A111	-65 ± 7	-39 ± 6	-131 ± 17	147 ± 12
A112	-63 ± 6	-42 ± 7	-136 ± 11	146 ± 15
L113	-66 ± 6	-38 ± 7	-123 ± 21	139 ± 20
G114	-64 ± 4	-41 ± 3	—	—
V115	-61 ± 3	-42 ± 5	—	—
A116	-62 ± 5	-37 ± 4	-62 ± 4	-39 ± 2
T117	-68 ± 8	-38 ± 7	-68 ± 8	-39 ± 6
A118	-64 ± 7	-39 ± 6	-61 ± 3	-43 ± 6
A119	-66 ± 4	-43 ± 4	-66 ± 8	-40 ± 7
Q120	-67 ± 6	-40 ± 7	-69 ± 6	-39 ± 8
V121	-68 ± 7	-41 ± 7	-64 ± 7	-41 ± 5
T122	-63 ± 4	-40 ± 10	-63 ± 4	-42 ± 7
A123	-60 ± 5	-38 ± 7	-64 ± 4	-37 ± 6
A124	-64 ± 5	-39 ± 9	-64 ± 6	-45 ± 4
V125	-61 ± 5	-44 ± 7	-68 ± 19	-40 ± 12
A126	-59 ± 4	-40 ± 6	—	—
L127	-75 ± 19	-36 ± 14	—	—

<sup>a</sup>The DOPC/DOPG values were predicted from the main set of chemical shifts.

three lipid membranes, POPC/POPG, DOPC/DOPG, and POPC, highlights the membrane-induced conformational polymorphism of FPK4. The  $\alpha$ -helical chemical shifts of the C-terminal half of the peptide are the same between the POPC/POPG and DOPC/DOPG membranes, whereas the  $\beta$ -strand chemical shifts of the N-terminal residues differ between the POPC and DOPC/DOPG membranes. For example, the chemical shifts of I108, A112, and L113 in the DOPC/DOPG membrane are intermediate between the corresponding chemical shifts in the POPC and POPC/POPG membranes (Figure 2c).

On the basis of the cross-peak intensities in the low-temperature 2D  $^{13}\text{C}$ – $^{13}\text{C}$  spectra, we quantified the  $\alpha$ -helical content of each residue (Table S1, Supporting Information). Residues up to L113 are less than 35%  $\alpha$ -helical, whereas residues A116–V125 are greater than 50% helical. The increasing helicity toward the C terminus was consistently observed for all labeled peptides, independent of minor variations in the hydration and salt content of the samples.

The TALOS+ predicted backbone ( $\varphi$ ,  $\psi$ ) torsion angles of the major conformer of DOPC/DOPG-bound FPK4 (Table 3) confirm the N-terminal  $\beta$ -strand and C-terminal  $\alpha$ -helical structures of the peptide. For this mixed conformation, oligomerization, if present, is expected to be parallel rather than antiparallel. This is consistent with the cross-peak pattern detected at long mixing times. The labeled residues within GVTAA- and IGALV-FPK4 lie at the two ends of the peptide. Thus, if antiparallel packing or a hairpinlike structure were present, we would observe inter-residue cross peaks between the N- and C-terminal residues. The 500 ms 2D spectra (Figure S2, Supporting Information) of these samples show only sequential inter-residue cross peaks such as G105–V106, T122–A123, I108–G109, and A112–L113 but no long-range cross peaks, thus ruling out antiparallel packing and the helical hairpin conformation.

**Depth of Insertion and Lipid Interaction of FPK4 in the DOPC/DOPG Membrane.** Since FPK4 adopts a surface-bound  $\beta$ -strand structure in neutral PC membranes<sup>52</sup> but an inserted  $\alpha$ -helical structure in the anionic POPC/POPG membrane, the topology of the partial  $\beta$ -strand peptide in the anionic DOPC/DOPG membrane is not immediately obvious. We thus measured the depth of the peptide in the DOPC/DOPG membrane, using both the LC-phase  $^1\text{H}$  spin diffusion experiment and the gel-phase experiment. By 100 ms, the 2D  $^1\text{H}$ – $^{13}\text{C}$  correlation spectra at 293 K (Figure S3, Supporting Information) showed clear cross peaks between lipid-chain protons and peptide  $^{13}\text{C}$  for both the  $\beta$ -strand and  $\alpha$ -helical residues, indicating that the entire peptide is inserted into the DOPC/DOPG membrane. This is confirmed by the fast lipid-to-peptide spin diffusion buildup rates for both conformations (Figure S3c, f, Supporting Information). More residue-specific depth information is obtained from the gel-phase spin diffusion spectra obtained at 243 K. By 4 ms, the peptide  $^1\text{H}$  cross section is already similar to the lipid  $^1\text{H}$  cross section (Figure 7a), indicating equilibration of the  $^1\text{H}$  magnetization among the peptide, lipid, and water. Similar to the POPC/POPG case, FPK4 has higher water/lipid cross-peak intensity ratios for the terminal residues than the central residues (Figure 7b, c), indicating that the peptide spans the bilayer thickness. But in contrast to the POPC/POPG-bound FPK4, the C-terminal  $\alpha$ -helical residues are significantly more exposed to water than the N-terminal  $\beta$ -strand residues (Figure 7c). The LC-phase spin diffusion spectra (Figure S3c, f, Supporting Information) also exhibit slightly faster lipid–peptide spin diffusion buildup rates for the N-terminal residues than the C-terminal residues. It is not fully clear whether it is the backbone conformation (helix versus strand) or the residue position (N or C termini) that causes the different insertion asymmetry between the POPC/POPG and DOPC/DOPG membranes. However, the minor  $\beta$ -strand conformation of the C-terminal A123 and A124 has lower water/lipid intensity ratios than the  $\alpha$ -helical counterpart, while the minor  $\alpha$ -helical conformation of the N-terminal L110 has higher water exposure than  $\beta$ -strand L110 (Figure 7c), suggesting that conformation may be the more important determinant of depth: the  $\beta$ -strand conformation is more deeply inserted than the  $\alpha$ -helical conformation into the DOPC/DOPG membrane.

To investigate whether FPK4 causes curvature and dehydration to the DOPC/DOPG membrane, we measured the static and MAS  $^{31}\text{P}$  spectra (Figure S4a, b, Supporting Information). FPK4 displayed little perturbation of the structure of the DOPC/DOPG membrane: the lamellar-bilayer powder pattern is retained, and the isotropic chemical shift is unchanged. However, the MAS isotropic line width is significantly broadened by the peptide (from 30 to 130 Hz), and the  $^{31}\text{P}$  transverse relaxation times of DOPC and DOPG decreased from 18.3 and 19.4 ms, respectively, for the peptide-free membrane to 2.4 and 2.0 ms for the peptide-bound membrane (Figure S4c, Supporting Information). Thus, the apparent  $^{31}\text{P}$  linewidths are largely homogeneous, and the fusion peptide slows down the lipid headgroup motion without changing its average conformation. Finally, the 2D  $^{31}\text{P}$ – $^1\text{H}$  correlation spectrum shows clear water–lipid cross peaks (Figure S4d, Supporting Information) for both DOPC and DOPG, indicating that FPK4 retains the hydration of the membrane surface.

The  $^{31}\text{P}$  MAS spectrum (Figure S4b, Supporting Information) exhibits a small isotropic peak at 2.2 ppm. This peak can be assigned to the phosphate buffer, since samples prepared in Tris or HEPES buffer did not show this peak (data not shown). We previously observed the same isotropic peak in static and MAS  $^{31}\text{P}$  spectra of FPK4-containing POPC and DMPC

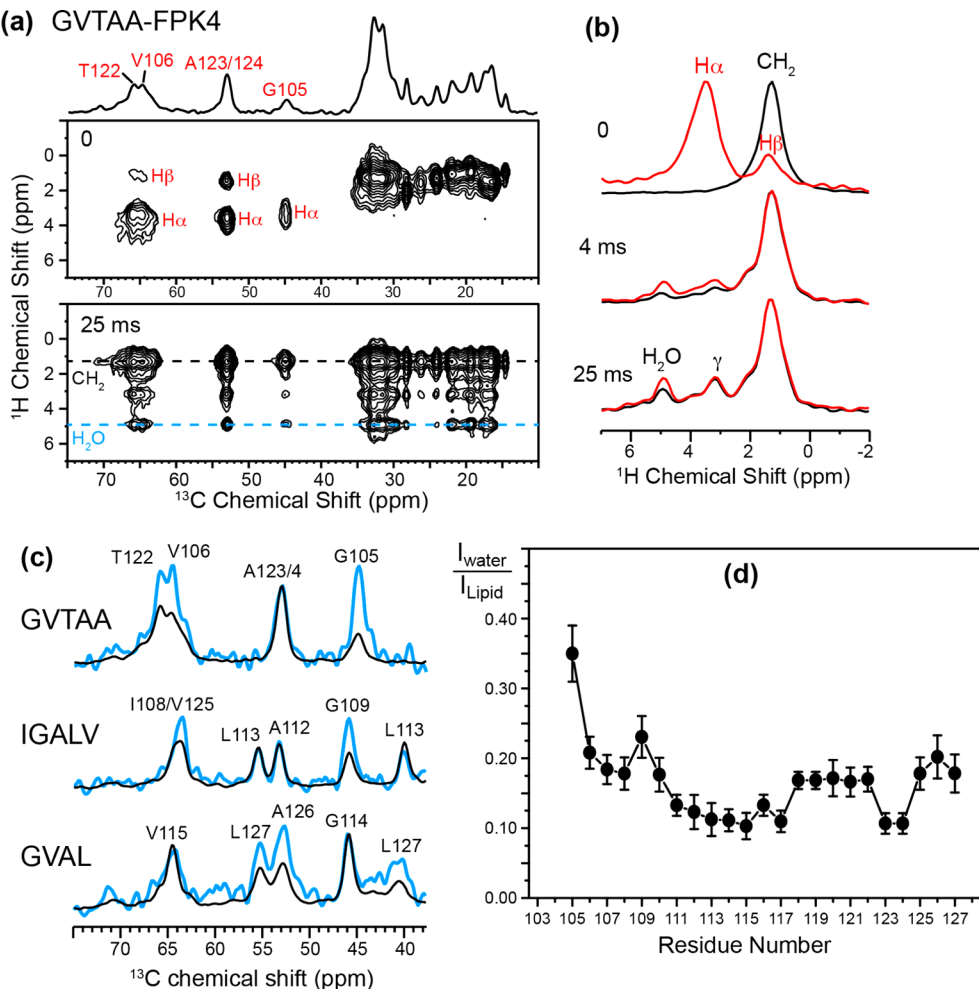


**Figure 4.** Depth of insertion of FPK4 in the POPC/POPG membrane from gel-phase spin diffusion. (a) Representative 2D spectra with 0 and 25 ms spin diffusion mixing at 258 K. (b) <sup>1</sup>H cross sections for the peptide C $\alpha$  peaks (red) and the lipid CH<sub>2</sub> peak (black). Already at 4 ms, the peptide and lipid <sup>1</sup>H cross sections have similar intensity patterns, indicating that the peptide is well inserted into the membrane. (c) <sup>13</sup>C cross sections extracted from the water (blue) and lipid CH<sub>2</sub> (black) <sup>1</sup>H chemical shifts from the 4 ms 2D spectra. The N- and C-terminal residues have higher water/lipid intensity ratios than the middle residues. (d) Water/lipid intensity ratios for all labeled sites.

membranes, and the peak intensity increased with the peptide concentration. The latter led to the erroneous conclusion that this peak resulted from a peptide-induced high-curvature isotropic phase.<sup>52</sup> We now attribute the concentration dependence of this <sup>31</sup>P peak to electrostatic attraction between the cationic Lys tag and the phosphate ions. Similar cases of phosphate buffer interactions with membrane peptides have been reported in the literature.<sup>63</sup> Thus, the  $\beta$ -strand FPK4 that binds to the surface of the POPC membrane does not cause curvature on the sub-10 nm scale. However, this does not exclude the possibility that the peptide may cause curvature on larger length scales of 50–100 nm, which would not manifest as a narrow peak in the static <sup>31</sup>P spectra.<sup>64</sup>

**FPK4 Conformation and Lipid Interaction in the DOPE Membrane.** To further investigate whether FPK4 induces membrane curvature, we studied the structure and lipid interactions of DOPE-bound FPK4. The small headgroup of DOPE and its disordered acyl chains create spontaneous negative curvature to the membrane, causing an inverse hexagonal phase (H<sub>II</sub>) in a wide temperature range. The DOPE phase diagram has been measured using NMR and X-ray diffraction,<sup>65,66</sup> and the lamellar (L <sub>$\alpha$</sub> )–H<sub>II</sub> transition temperature ( $T_h$ ) is known to depend on the hydration: above  $\sim$ 16 water molecules per lipid, the

membrane converts to the H<sub>II</sub> phase by  $\sim$ 283 K. If FPK4 causes membrane curvature, then  $T_h$  will be affected: positive curvature generation by the peptide increases  $T_h$  while negative curvature generation lowers the transition temperature.

Figure 8 shows the static <sup>31</sup>P spectra of DOPE membranes without and with FPK4 from 273 to 313 K. At 273 K, pure DOPE membrane shows an L <sub>$\alpha$</sub> -phase powder pattern with a chemical shift anisotropy span of +44.5 ppm. Above 273 K, the <sup>31</sup>P spectrum shows increasing intensities of a narrower line shape with a span of  $\sim$ 21.5 ppm, which is inverted from the L <sub>$\alpha$</sub>  line shape around the isotropic <sup>31</sup>P chemical shift. This inverted and halved CSA is the signature of the hexagonal phase.<sup>67</sup> The pure DOPE membrane fully converted to the H<sub>II</sub> phase by 283 K (Figure 8a), consistent with the reported  $T_h$  value.<sup>65,66</sup> Upon FPK4 binding, the L <sub>$\alpha$</sub> –H<sub>II</sub> transition shifted to higher temperatures and was complete only by  $\sim$ 293 K, indicating that FPK4 exerted positive membrane curvature. In addition, an isotropic peak appeared in the spectra (Figure 8b). In principle, this isotropic peak can result from either micelles or cubic phases. However, micelle formation by the long-chain DOPE is unlikely. Moreover, small-angle X-ray diffraction data of DOPE containing the HA fusion peptide indicated the presence of inverted bicontinuous cubic phases as well as an increase of the L <sub>$\alpha$</sub> –H<sub>II</sub> transition temperature,<sup>68</sup> and

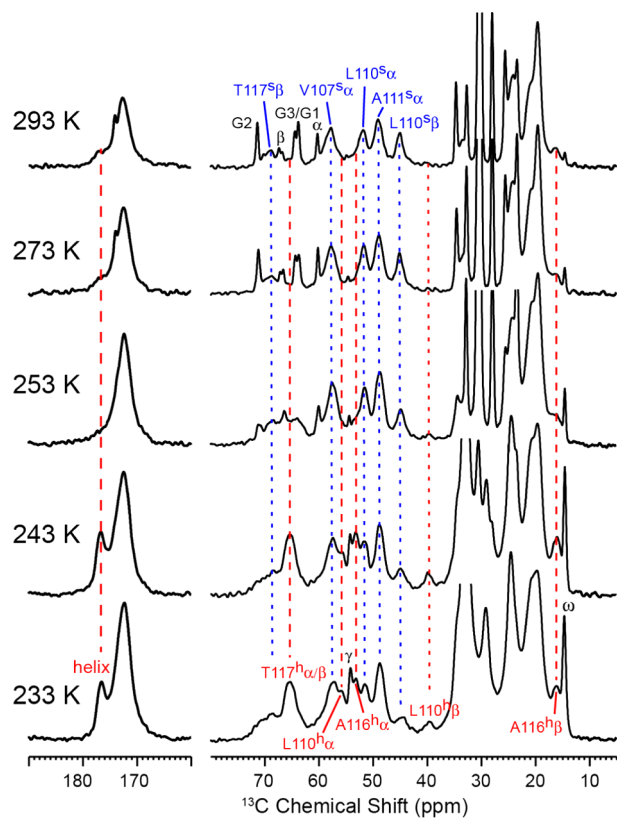


**Figure 5.** Representative 1D  $^{13}\text{C}$  CP MAS spectra of DOPC/DOPG-bound FPK4 as a function of temperature. The VLAAT-FPK4 spectra are shown. At high temperature, mainly  $\beta$ -strand chemical shifts (blue dotted lines) are observed, while at low temperature, both  $\alpha$ -helical (red dashed lines) and  $\beta$ -strand chemical shifts are detected.

independent MD simulations also predicted the same effect.<sup>46</sup> Thus, the isotropic  $^{31}\text{P}$  peak seen here is most likely due to cubic-phase formation in the DOPE membrane, which suggests that the PIV5 fusion peptide causes both positive and negative curvatures; that is, the peptide generates negative Gaussian curvature. Also known as saddle-splay curvature, negative Gaussian curvature results from the product of positive and negative principal curvatures and is present at membrane pores and protrusions formed during membrane budding and scission.<sup>69,70</sup>

The equilibrium FPK4 conformation in the DOPE membrane is predominantly  $\beta$ -strand, after the transient existence of a mixed strand/helix conformation (Figure 9a, b). The  $\beta$ -strand shows clear cross peaks with lipid  $\text{CH}_2$  protons in the 2D  $^1\text{H}$ – $^{13}\text{C}$  correlation spectra (Figure 9c), indicating that the peptide is embedded in the hydrophobic region of the hexagonal-phase cylinders (Figure 10e). The 2D  $^{31}\text{P}$ – $^1\text{H}$  correlation spectrum of the FPK4-bound DOPE membrane shows a much weaker water– $^{31}\text{P}$  cross peak than the peptide-free membrane (Figure 8c, d), indicating that the  $\beta$ -strand FPK4 dehydrates the DOPE membrane in addition to causing curvature to this membrane.

## DISCUSSION

### Conformational Polymorphism of the PIV5 Fusion Peptide.

The present solid-state NMR data indicate at least four distinct conformations and membrane topologies of the PIV5 fusion peptide. In the POPC/POPG membrane, the peptide adopts a membrane-spanning  $\alpha$ -helical conformation (Figure 10a). The POPC/POPG membrane has a hydrophobic thickness of  $\sim 27 \text{ \AA}$  at  $30^\circ\text{C}$  based on X-ray scattering data.<sup>71,72</sup> The full

$\alpha$ -helix has a length of  $\sim 34 \text{ \AA}$  from G105 to L127  $\text{C}\alpha$  based on the TALOS+ structural model. Thus, the helix may be tilted by  $35\text{--}40^\circ$  to achieve optimal hydrophobic match between the POPC/POPG bilayer thickness and the peptide length.

In the DOPC/DOPG membrane, FPK4 adopts a mixed conformation with an N-terminal  $\beta$ -strand (residues 105–113) and a C-terminal  $\alpha$ -helix (residues 116–125). The  $\beta$ -strand is more deeply inserted than the  $\alpha$ -helical segment. No chemical shift constraints were measured for residues G114, A115, A126, and L127. The current structural model assumed A126–L127 to be similarly helical as in the POPC/POPG-bound FPK4 and G114 and A115 to be random coil due to its position near a likely bend (see below). The overall dimension of the mixed helix/strand conformation is not known without long-range distance constraints. However, since the  $\beta$ -strand is much more extended than the  $\alpha$ -helix, the peptide is likely to be significantly tilted to match the hydrophobic thickness of the DOPC/DOPG bilayer, which is similar to that of the POPC/POPG bilayer.<sup>71,72</sup> In the DOPE membrane (Figure 10e), the chemical shift constraints suggest a predominantly  $\beta$ -strand peptide, which is inserted into the hydrophobic region between the lipid cylinders. Finally, FPK4 adopts a surface-bound  $\beta$ -strand structure in neutral POPC and DMPC membranes, as we showed previously.<sup>52</sup>

The four conformations and topologies of FPK4 suggest several principles for the influence of the lipid membrane on the fusion peptide structure. First, while the entire sequence of the fusion peptide is capable of conformational polymorphism, the C terminus has a higher propensity for the  $\alpha$ -helical structure. Second, anionic membranes promote the  $\alpha$ -helical conformation, as shown by the difference between the POPC/POPG membrane and the POPC membrane and by the difference between DOPC/DOPG and DOPE membranes. Third, more disordered membranes shift the peptide conformational equilibrium toward  $\beta$ -strand, as shown by the difference between the POPC/POPG and DOPC/DOPG membranes. The third observation, while initially unexpected, can in fact be understood by the fact that lipid unsaturation not only changes membrane dynamics but also membrane curvature. Cone-shaped lipids (with negative intrinsic curvature) such as oleic acids, *cis*-unsaturated lipids, and phosphatidylethanolamine promote stalk formation, whereas inverted-cone shaped lipids (with positive curvature) such as lysophosphocholine inhibit fusion by preventing stalk formation.<sup>73–75</sup> Thus, the more unsaturated DOPC/DOPG lipids change the membrane curvature in addition to membrane dynamics compared to the POPC/POPG lipids. The higher  $\beta$ -strand content of the fusion peptide in the DOPC/DOPG membrane thus suggests that the  $\beta$ -strand structure may be the active form in hemifusion intermediates.

Our chemical shift analysis indicates that the PIV5 fusion peptide has a higher conformational disorder in the middle of the sequence, near G114–T117. This region is not only the transition point between the strand and helix segments in the DOPC/DOPG-bound peptide but also has multiple conformations and residual dynamics in the POPC/POPG membrane. The prefusion crystal structures of several viral fusion proteins and the NMR structures of other fusion peptides suggest that conformational disorder in the middle of fusion peptide domains may be general. For example, in the uncleaved PIV5 F protein,<sup>22</sup> the C-terminal part (A118–V128) of the buried fusion peptide shows an  $\alpha$ -helical structure extended from HRA, whereas the N-terminal part (F103–T117) has a mixed conformation of random coil (F103–I108),  $\alpha$ -helix (G109–L113), and  $\beta$ -strand (V115–A116) (Figure 10b). T117 is the hinge between the

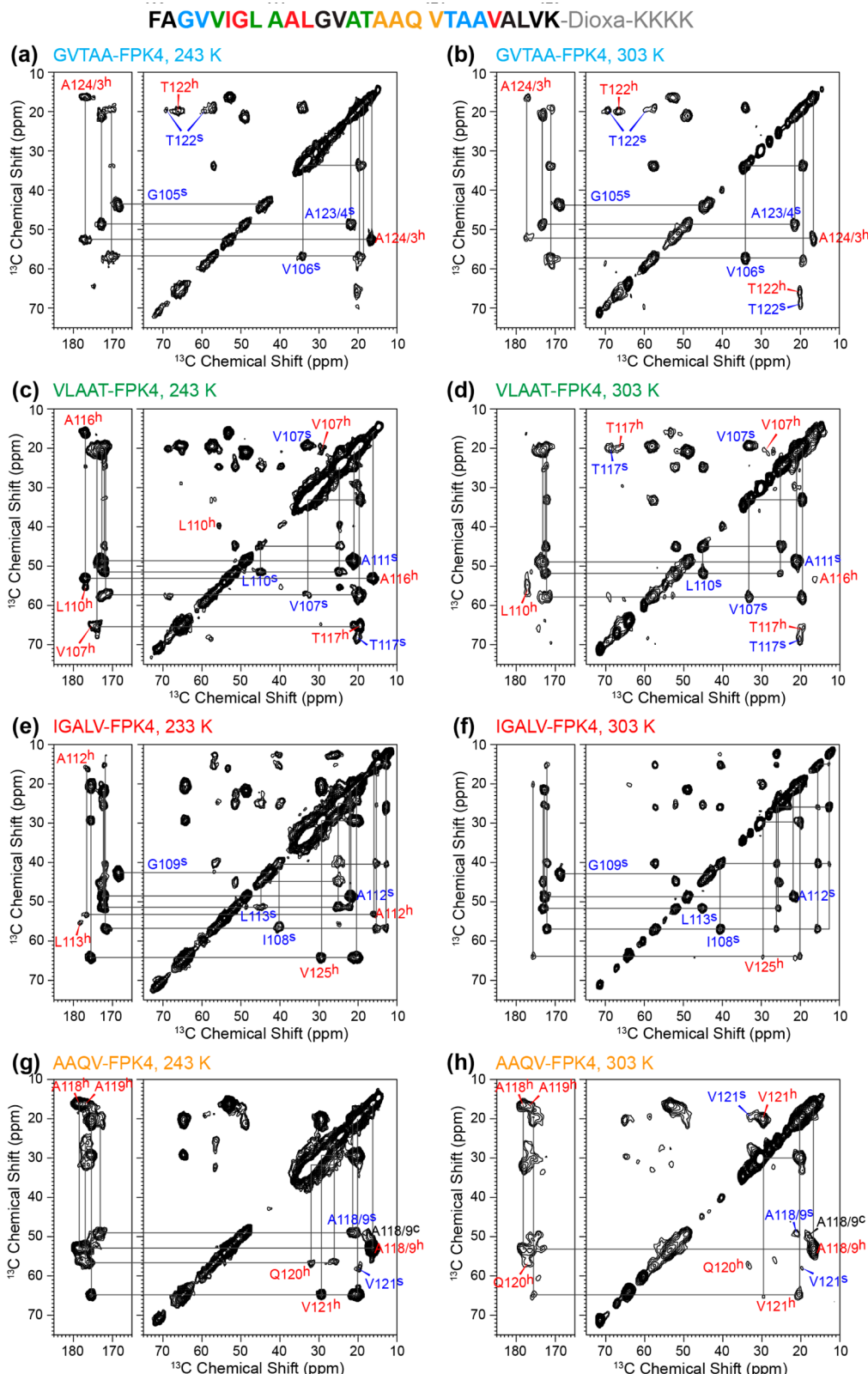


**Figure 6.** 2D  $^{13}\text{C}$ – $^{13}\text{C}$  correlation spectra of DOPC/DOPG-bound FPK4 in the gel phase (233 or 243 K, left column) and the LC phase (303 K, right column). (a, b) GVTAA-FPK4 spectra. (c, d) VLAAT-FPK4 spectra. (e, f) IGALV-FPK4 spectra. (g, h) AAQV-FPK4 spectra. At both temperatures, many residues show mixed  $\alpha$ -helical and  $\beta$ -strand chemical shifts.

N- and C-terminal halves. After cleavage,<sup>21</sup> the first four residues of the FP undergo an orientational change while the other residues are mostly unaffected. In the prefusion HA crystal structures, the FP is unstructured in both uncleaved and cleaved

states,<sup>76,77</sup> but the N-terminal segment undergoes a large-amplitude rotation with respect to the rest of the protein after cleavage (Figure 10c). Isolated HA fusion peptides bound to DPC micelles exhibit  $\alpha$ -helical conformations, but the middle of the

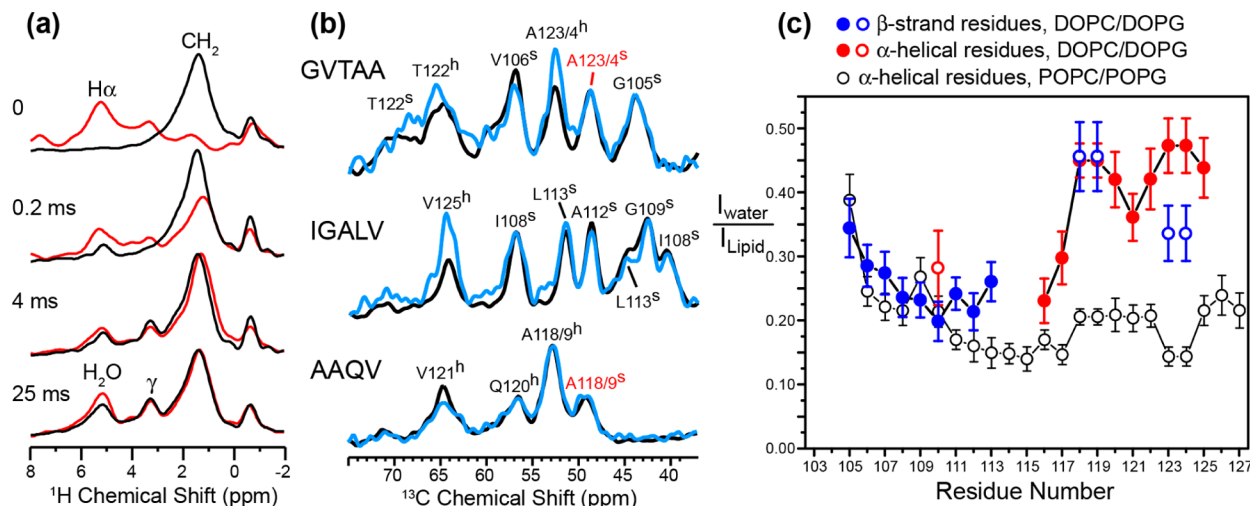


**Figure 7.** Depth of insertion of FPK4 in the DOPC/DOPG membrane from gel-phase spin diffusion spectra measured at 243 K. (a)  $^1\text{H}$  cross sections of the peptide C $\alpha$  peaks (red) and lipid CH<sub>2</sub> peak (black). By 4 ms, the peptide and lipid signals have equilibrated, indicating that the peptide is well inserted into the membrane. (b)  $^{13}\text{C}$  cross sections from the water (blue) and lipid CH<sub>2</sub> (black)  $^1\text{H}$  chemical shifts of the 4 ms 2D spectra. The C-terminal  $\alpha$ -helical residues have higher water cross peaks than the N-terminal  $\beta$ -strand residues, and the  $\alpha$ -helical A123/A124 have higher water cross peaks than the  $\beta$ -strand A123/A124. (c) Water/lipid intensity ratios of all labeled residues in the DOPC/DOPG membrane (blue and red symbols). The  $\beta$ -strand residues have lower water exposure than the  $\alpha$ -helical residues. Open symbols indicate the minor conformation. For comparison, the POPC/POPG-bound FPK4 data are also shown (black open symbols).

peptide is disordered and forms the bend of the helical hairpin in the 23-residue construct<sup>29</sup> and the bend of the boomerang structure in the 20-residue construct.<sup>24</sup> The exact significance of this mid-domain disorder for membrane fusion is not clear, but we speculate that the disorder may be useful for controlling oligomerization, the degree of peptide insertion into the membrane, and membrane hydration. For example, if the  $\beta$ -sheet conformation is indeed more effective in dehydrating the lipid membrane than the  $\alpha$ -helical conformation, as suggested by the current DOPE data and the previous POPC and DMPC data, then a mixed strand/helix conformation may be useful for dehydrating one of the two surfaces of the lipid bilayer.

Mutagenesis data of the fusion peptide domain of the PIV5 F protein indicated a competition between protein transport, surface expression, and membrane fusion, but the N-terminal residues F103–V115 appear to be more important for membrane fusion than other functions.<sup>6</sup> Mutations of G105, G109, and G114 to Ala reduced protein expression but increased membrane fusion. G109A and G114A mutants showed 25% lower expression levels but 10-fold higher membrane fusion than the wild-type protein.<sup>6</sup> While fusion peptides are generally rich in Gly and Ala residues,<sup>50,58,78</sup> in PIV5 FP, all three Gly residues are located in the N-terminal region while over half of the Ala residues are located in the C-terminal region. In contrast, HA and HIV fusion peptides have a more uniform distribution of Gly residues. The high Gly content of the N-terminal half of the PIV5 fusion peptide may be one of the reasons for the stronger  $\beta$ -strand propensity of the N-terminal half. Meanwhile, the helix propensity of the C-terminal segment may be related to the neighboring  $\alpha$ -helical HRA domain, as seen in the postfusion crystal structure of PIV5 F, which shows  $\alpha$ -helical T122–V128 in the FP domain.<sup>14</sup> Since the N-terminal domain is more important for membrane fusion and has a stronger propensity for the  $\beta$ -strand conformation, the  $\beta$ -strand conformation may be more critical for membrane fusion. This is also consistent with the ability of the  $\beta$ -strand conformation in causing membrane dehydration, as discussed below.

**Curvature Generation and Membrane Dehydration by the PIV5 Fusion Peptide.** Static  $^{31}\text{P}$  NMR spectra indicate that the PIV5 fusion peptide neither causes curvature nor dehydration to the POPC/POPG and DOPC/DOPG membranes but causes curvature to the DOPE membrane. The peptide increased the  $L_{\alpha}$ – $H_{\text{II}}$  transition temperature by about 10 K and generated a small amount of an isotropic phase. We attribute this signal to a cubic phase, which would suggest that the FP promotes negative Gaussian curvature.

Increasing experimental evidence and simulations indicate that generation of negative Gaussian curvature may be a common property of viral fusion peptides. Recent small-angle X-ray diffraction data<sup>68</sup> of the HA fusion peptide in methylated DOPE showed that the peptide shifted the  $L_{\alpha}$ – $H_{\text{II}}$  phase transition to higher temperatures and additionally promoted the formation of inverted bicontinuous cubic phases,  $lm3m$  and  $Pn3m$ , which possess negative Gaussian curvature. This result revises earlier literature that concluded that the HA fusion peptide promoted only negative curvature.<sup>79,80</sup> These earlier studies were based on differential scanning calorimetry experiments, which may not be able to resolve the cubic phases from the  $L_{\alpha}$  and  $H_{\text{II}}$  phases, and on  $^{31}\text{P}$  NMR spectra that showed clear isotropic peaks but poor-sensitivity powder patterns that cannot be definitively assigned to either the  $L_{\alpha}$  phase or the  $H_{\text{II}}$  phase. Therefore, these earlier data cannot be interpreted as stabilization of the  $H_{\text{II}}$  phase by the HA fusion peptide,<sup>33,50</sup> but they do indicate the generation of an isotropic phase, which is consistent with cubic-phase formation. Molecular dynamics simulations of membranes containing the HA fusion peptide indicate that the peptide systematically shifted the lipid phase diagram toward more positive mean curvature and bicontinuous cubic phases.<sup>46</sup> For the HIV gp41 fusion peptide,  $^{31}\text{P}$  NMR spectra and cryo-TEM micrographs<sup>81,82</sup> of DOPE-containing lipid membranes showed the presence of an isotropic phase. Thus, all reliable evidence converges to indicate that influenza, HIV, and PIV5 fusion peptides cause negative Gaussian curvature to PE-rich membranes. On the basis of the intensity of the  $^{31}\text{P}$  isotropic peak, the PIV5 FPK4 construct used

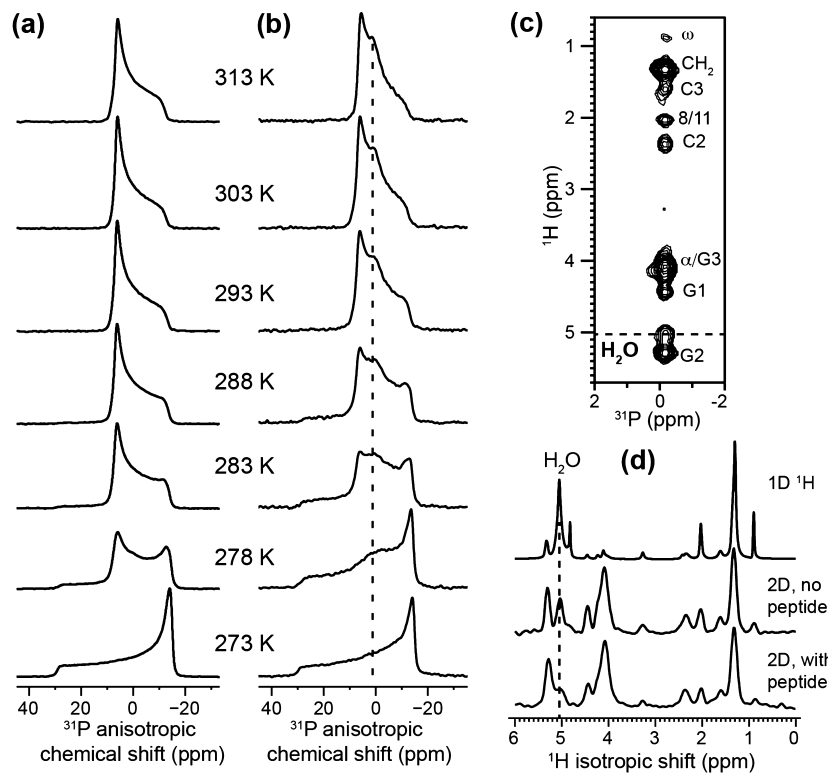


**Figure 8.** FPK4 interaction with the DOPE membrane. (a, b) Static  $^{31}\text{P}$  spectra of the membrane without (a) and with (b) FPK4 from 273 to 313 K. FPK4 increased the  $\text{L}_{\alpha}$ -to- $\text{H}_{\text{II}}$  phase transition temperature and caused a small isotropic peak. (c) 2D  $^{31}\text{P}$ - $^1\text{H}$  correlation spectrum of FPK4-bound DOPE membrane with a spin diffusion mixing time of 225 ms. (d)  $^1\text{H}$  cross sections from the 2D  $^{31}\text{P}$ - $^1\text{H}$  spectra of peptide-free and peptide-bound DOPE membranes, compared with the 1D  $^1\text{H}$  single-pulse spectrum (top). The FPK4-bound DOPE membrane has a much weaker water- $^{31}\text{P}$  cross peak than the peptide-free membrane.

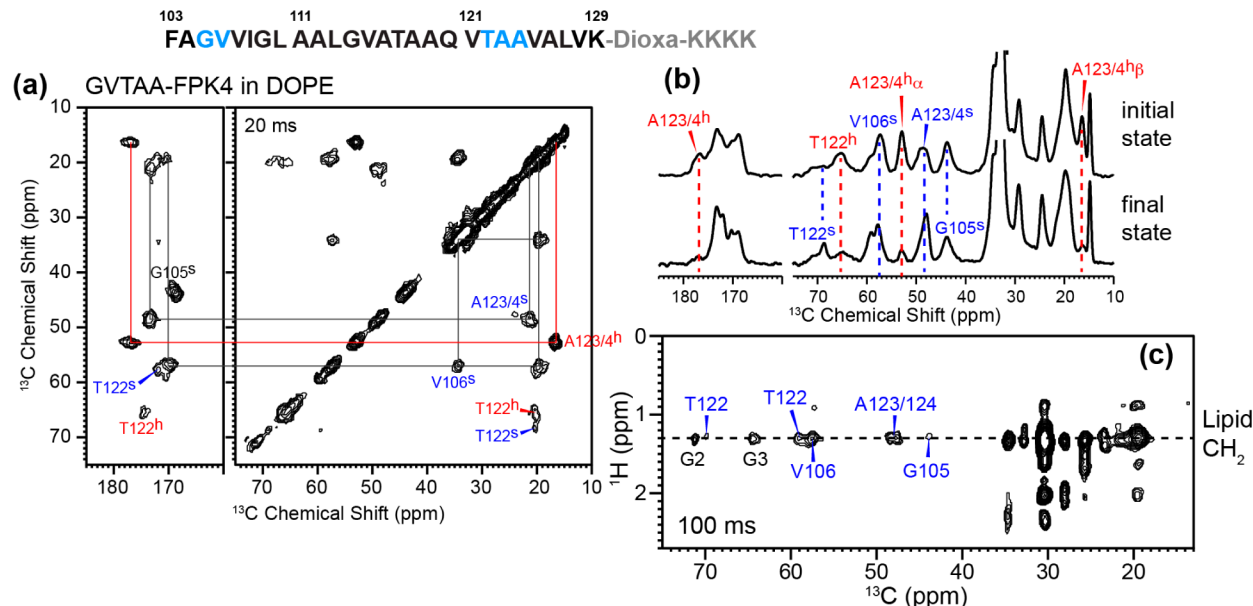


**Figure 9.** Conformation and depth of FPK4 in the DOPE membrane. (a) 2D  $^{13}\text{C}$ - $^{13}\text{C}$  correlation spectrum of a fresh GVTAA-FPK4 sample at 243 K. The peptide exhibits both helix and strand signals. (b)  $^{13}\text{C}$  CP-MAS spectra of the initial and equilibrated GVTAA-FPK4 at 246 K. At equilibrium, most residues exhibit  $\beta$ -strand chemical shifts. (c) 100 ms 2D  $^{13}\text{C}$ - $^1\text{H}$  correlation spectrum at 293 K, in the  $\text{H}_{\text{II}}$  phase membrane. Lipid-peptide cross peaks are observed, indicating that the  $\beta$ -strand peptide is inserted into the hydrophobic region of the DOPE membrane.

here has weaker curvature-generating ability than the influenza and HIV fusion peptides.

In addition to generating membrane curvature, FPK4 also partially dehydrated the DOPE membrane (Figure 8c, d). For the  $\text{H}_{\text{II}}$ -phase DOPE, this means a reduction of the water-core

diameter of the cylinders. Figure 10e depicts the hexagonal cylinders, where the relative dimensions of the water pore and the hydrophobic chains match the values reported from X-ray diffraction data of DOPE<sup>66</sup> at 15–18 water molecules per lipid, which is the hydration level of the FPK4-containing DOPE

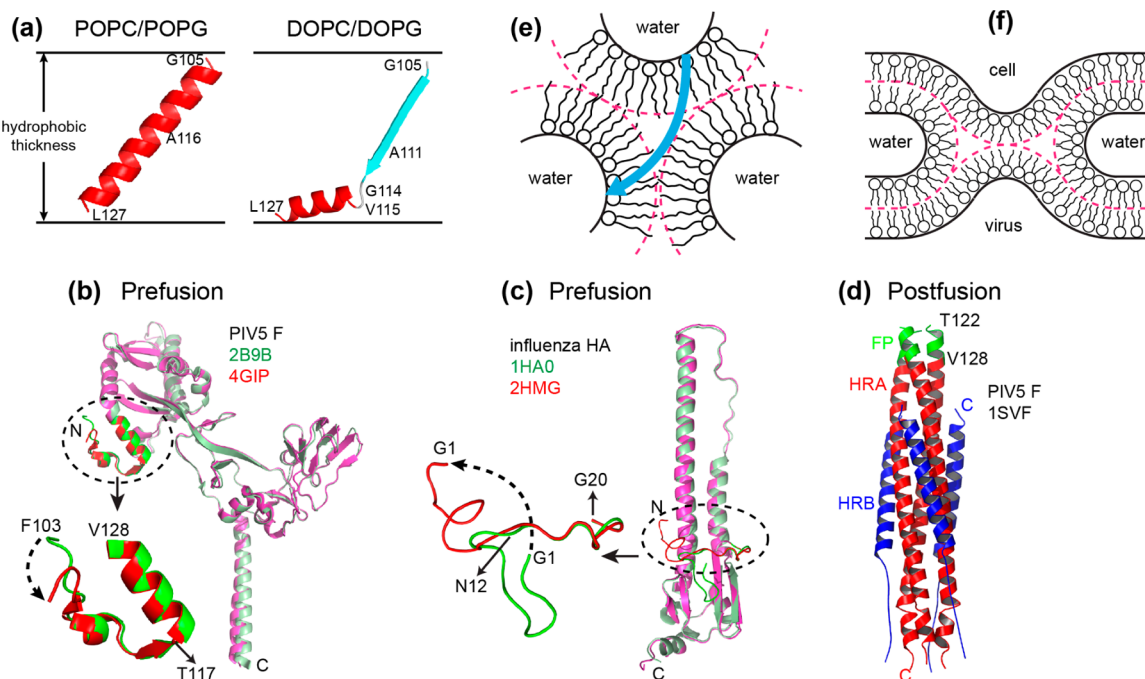


**Figure 10.** PIV5 fusion peptide conformations in lipid membranes from solid-state NMR and outside the membrane from crystal structures. (a) Fusion peptide is fully  $\alpha$ -helical in POPC/POPG bilayers but adopts a mixed strand/helix conformation in DOPC/DOPG bilayers. The peptide is inserted into both membranes, but the depicted tilt angle is hypothetical. The structures were built using  $(\varphi, \psi)$  torsion angles predicted by TALOS+. (b) Prefusion crystal structures of the PIV5 F protein in the uncleaved (green)<sup>22</sup> and cleaved (red)<sup>21</sup> states. The fusion peptide domain has similar conformations before and after cleavage and has a bend near T117. (c) Prefusion crystal structures of the influenza HA in the uncleaved (green)<sup>76</sup> and cleaved (red)<sup>77</sup> states. The N-terminal half of the fusion peptide is rotated around N12 before and after cleavage. (d) Postfusion crystal structure of the PIV5 F HRA/HRB complex.<sup>14</sup> Seven residues (T122–V128) of the fusion peptide are detected and show  $\alpha$ -helical structure extended from HRA. (e) Schematic of the PIV5 fusion peptide conformation in the DOPE membrane. The lipid cylinders and water radius are drawn to scale using 15–18 water molecules per lipid based on the DOPE phase diagram.<sup>65,66</sup> (f) The hemifusion stalk intermediate showing both negative and positive membrane curvatures and dehydration between two opposing bilayers. Dashed lines indicate the middle of two lipid leaflets.

membrane. At this hydration, the water channel radius is  $\sim 19$  Å, while the distance between the centers of two cylinders in adjacent layers ( $D_{\text{hex}}$ ) is  $\sim 70$  Å, whose hydrophobic portion ( $\sim 32$  Å) is traversed by the  $\beta$ -strand FPK4. This peptide location is consistent with X-ray scattering data<sup>83</sup> that showed that the HIV fusion peptide increased the  $D_{\text{hex}}$  value of DOPE at peptide concentrations above 2 mol %. The increased hexagonal spacing results from a compensatory effect of an increased hydrocarbon volume, which implicates the HIV fusion peptide to be embedded in the hydrocarbon region, and a decreased water volume, which agrees with the dehydration seen in the current 2D  $^{31}\text{P}$ – $^1\text{H}$  correlation spectra of the DOPE membrane. Thus, the PIV5 and HIV fusion peptides exert similar changes to the DOPE membrane. The cross section of the inverse-hexagonal phase DOPE, in which the opposed lipid chains of different cylinders experience negative curvature (Figure 10e), is similar but not identical to the cross section of the hemifusion stalk intermediate (Figure 10f),<sup>11,47</sup> since the latter also contains lipids experiencing positive curvature. The hemifusion stalk is topologically more similar to inverted bicontinuous cubic phases,<sup>84,85</sup> which are the likely cause of the isotropic peak in the  $^{31}\text{P}$  spectra. The lipids that experience positive curvature in the cubic phase should correspond to lipids in the distal leaflet of the opposing membranes.

## CONCLUSION

On the basis of the conformation, topology, and lipid and water interactions of PIV5 FPK4 in the four lipid membranes obtained from solid-state NMR, we propose the following relations between the FP structure and viral membrane fusion. When the FP is released from the globular head of the F protein, it inserts into the

target cell membrane in an  $\alpha$ -helical structure. As the protein rearranges its structure and HRA forms a coiled-coil trimer in the prehairpin intermediate, the fusion peptides of the three proteins interact in the cell membrane to form a homotrimer. When several trimers cluster in regions of the membrane containing high concentrations of unsaturated lipids with their ensuing negative intrinsic curvature, the Gly-rich N-terminal half of the fusion peptide converts to a  $\beta$ -strand conformation, which dehydrates the membrane surface and exerts negative Gaussian curvature to the membrane. At this point, depending on the local lipid composition, the fusion peptide may be partially  $\beta$ -strand (in PC-rich membranes) or fully  $\beta$ -strand (in PE-rich membranes), and the peptide is well inserted unless the local membrane composition is predominantly neutral PC. When the water-soluble ectodomain completes its conformational change to a six-helix bundle, the FP and TM domains are forced into close proximity, which may revert the fusion peptide to the  $\alpha$ -helical conformation, which may in turn reduce membrane curvature and increase membrane hydration. Multiple lines of evidence obtained here suggest the  $\beta$ -strand conformation of the fusion peptide to be the most relevant structure in hemifusion intermediates, responsible for remodeling the membrane<sup>83</sup> to acquire the curvature and low hydration necessary for progression to complete fusion.

## ASSOCIATED CONTENT

### Supporting Information

Additional 2D spectra and a table of residue-specific helicity of FPK4. This material is available free of charge via the Internet at <http://pubs.acs.org>.

## AUTHOR INFORMATION

### Corresponding Author

mhong@iastate.edu

### Notes

The authors declare no competing financial interest.

## ACKNOWLEDGMENTS

This work is funded by NIH grant GM066976 to M.H.

## REFERENCES

- (1) Fields, C. G.; Lloyd, D. H.; Macdonald, R. L.; Ottenson, K. M.; Nobel, R. L. *Peptide Res.* **1991**, *4*, 95.
- (2) Chang, A.; Dutch, R. E. *Viruses* **2012**, *4*, 613.
- (3) Dutch, R. E. *PLoS Pathog.* **2010**, *6*, e1000881.
- (4) Lamb, R. A.; Jardetzky, T. S. *Curr. Opin. Struct. Biol.* **2007**, *17*, 427.
- (5) Russell, C. J.; Luque, L. E. *Trends Microbiol.* **2006**, *14*, 243.
- (6) Horvath, C. M.; Lamb, R. A. *J. Virol.* **1992**, *66*, 2443.
- (7) Russell, C. J.; Jardetzky, T. S.; Lamb, R. A. *J. Virol.* **2004**, *78*, 13727.
- (8) Bissonnette, M. L.; Donald, J. E.; DeGrado, W. F.; Jardetzky, T. S.; Lamb, R. A. *J. Mol. Biol.* **2009**, *386*, 14.
- (9) Baquero, E.; Albertini, A. A.; Vachette, P.; Lepault, J.; Bressanelli, S.; Gaudin, Y. *Curr. Opin. Virol.* **2013**, *3*, 143.
- (10) Weissenhorn, W.; Hinz, A.; Gaudin, Y. *FEBS Lett.* **2007**, *581*, 2150.
- (11) White, J. M.; Delos, S. E.; Brecher, M.; Schornberg, K. *Crit. Rev. Biochem. Mol. Biol.* **2008**, *43*, 189.
- (12) Lamb, R. A.; Paterson, R. G.; Jardetzky, T. S. *Virology* **2006**, *344*, 30.
- (13) Harrison, S. C. *Nat. Struct. Mol. Biol.* **2008**, *15*, 690.
- (14) Baker, K. A.; Dutch, R. E.; Lamb, R. A.; Jardetzky, T. S. *Mol. Cell* **1999**, *3*, 309.
- (15) Chan, D. C.; Kim, P. S. *Cell* **1998**, *93*, 681.
- (16) McLellan, J. S.; Yang, Y.; Graham, B. S.; Kwong, P. D. *J. Virol.* **2011**, *85*, 7788.
- (17) Swanson, K.; Wen, X.; Leser, G. P.; Paterson, R. G.; Lamb, R. A.; Jardetzky, T. S. *Virology* **2010**, *402*, 372.
- (18) Tan, K.; Liu, J.; Wang, J.; Shen, S.; Lu, M. *Proc. Natl. Acad. Sci. U.S.A.* **1997**, *94*, 12303.
- (19) Yin, H. S.; Paterson, R. G.; Wen, X.; Lamb, R. A.; Jardetzky, T. S. *Proc. Natl. Acad. Sci. U.S.A.* **2005**, *102*, 9288.
- (20) Zhao, X.; Singh, M.; Malashkevich, V. N.; Kim, P. S. *Proc. Natl. Acad. Sci. U.S.A.* **2000**, *97*, 14172.
- (21) Welch, B. D.; Liu, Y.; Kors, C. A.; Leser, G. P.; Jardetzky, T. S.; Lamb, R. A. *Proc. Natl. Acad. Sci. U.S.A.* **2012**, *109*, 16672.
- (22) Yin, H. S.; Wen, X.; Paterson, R. G.; Lamb, R. A.; Jardetzky, T. S. *Nature* **2006**, *439*, 38.
- (23) Kim, Y. H.; Donald, J. E.; Grigoryan, G.; Leser, G. P.; Fadeev, A. Y.; Lamb, R. A.; DeGrado, W. F. *Proc. Natl. Acad. Sci. U.S.A.* **2011**, *108*, 20992.
- (24) Han, X.; Bushweller, J. H.; Cafiso, D. S.; Tamm, L. K. *Nat. Struct. Biol.* **2001**, *8*, 715.
- (25) Jaroniec, C. P.; Kaufman, J. D.; Stahl, S. J.; Viard, M.; Blumenthal, R.; Wingfield, P. T.; Bax, A. *Biochemistry* **2005**, *44*, 16167.
- (26) Lai, A. L.; Tamm, L. K. *J. Biol. Chem.* **2010**, *285*, 37467.
- (27) Li, Y.; Han, X.; Lai, A. L.; Bushweller, J. H.; Cafiso, D. S.; Tamm, L. K. *J. Virol.* **2005**, *79*, 12065.
- (28) Li, Y.; Tamm, L. K. *Biophys. J.* **2007**, *93*, 876.
- (29) Lorieau, J. L.; Louis, J. M.; Bax, A. *Proc. Natl. Acad. Sci. U.S.A.* **2010**, *107*, 11341.
- (30) Lorieau, J. L.; Louis, J. M.; Schwieters, C. D.; Bax, A. *Proc. Natl. Acad. Sci. U.S.A.* **2012**, *109*, 19994.
- (31) Lai, A. L.; Tamm, L. K. *J. Biol. Chem.* **2007**, *282*, 23946.
- (32) Tamm, L. K.; Lai, A. L.; Li, Y. *Biochim. Biophys. Acta* **2007**, *1768*, 3052.
- (33) Epand, R. M. *Biochim. Biophys. Acta* **2003**, *1614*, 116.
- (34) Li, Y.; Han, X.; Tamm, L. K. *Biochemistry* **2003**, *42*, 7245.
- (35) Sun, Y.; Weliky, D. P. *J. Am. Chem. Soc.* **2009**, *131*, 13228.
- (36) Lorieau, J. L.; Louis, J. M.; Bax, A. *Biopolymers* **2013**, *99*, 189.
- (37) Gordon, L. M.; Mobley, P. W.; Lee, W.; Eskandari, S.; Kaznessis, Y. N.; Sherman, M. A.; Waring, A. J. *Protein Sci.* **2004**, *13*, 1012.
- (38) Qiang, W.; Bodner, M. L.; Weliky, D. P. *J. Am. Chem. Soc.* **2008**, *130*, 5459.
- (39) Qiang, W.; Sun, Y.; Weliky, D. P. *Proc. Natl. Acad. Sci. U.S.A.* **2009**, *106*, 15314.
- (40) Lai, A. L.; Moorthy, A. E.; Li, Y.; Tamm, L. K. *J. Mol. Biol.* **2012**, *418*, 3.
- (41) Gordon, L. M.; Mobley, P. W.; Pilpa, R.; Sherman, M. A.; Waring, A. J. *Biochim. Biophys. Acta* **2002**, *1559*, 96.
- (42) Rafalski, M.; Lear, J. D.; DeGrado, W. F. *Biochemistry* **1990**, *29*, 7917.
- (43) Saez-Cirion, A.; Nieva, J. L. *Biochim. Biophys. Acta* **2002**, *1564*, 57.
- (44) Gabrys, C. M.; Qiang, W.; Sun, Y.; Xie, L.; Schmick, S. D.; Weliky, D. P. *J. Phys. Chem. A* **2013**, *117*, 9848.
- (45) Hong, M.; Zhang, Y.; Hu, F. *Annu. Rev. Phys. Chem.* **2012**, *63*, 1.
- (46) Fuhrmans, M.; Marrink, S. J. *J. Am. Chem. Soc.* **2012**, *134*, 1543.
- (47) Siegel, D. P. *Biophys. J.* **1999**, *76*, 291.
- (48) Kasson, P. M.; Pande, V. S. *PLoS Comput. Biol.* **2007**, *3*, e220.
- (49) Chernomordik, L. V.; Kozlov, M. M. *Cell* **2005**, *123*, 375.
- (50) Tamm, L. K.; Han, X. *Biosci. Rep.* **2000**, *20*, 501.
- (51) Siegel, D. P.; Epand, R. M. *Biochim. Biophys. Acta* **2000**, *1468*, 87.
- (52) Yao, H.; Hong, M. *J. Mol. Biol.* **2013**, *425*, 563.
- (53) Takegoshi, K.; Nakamura, S.; Terao, T. *Chem. Phys. Lett.* **2001**, *344*, 631.
- (54) Hong, M.; Griffin, R. G. *J. Am. Chem. Soc.* **1998**, *120*, 7113.
- (55) Huster, D.; Yao, X. L.; Hong, M. *J. Am. Chem. Soc.* **2002**, *124*, 874.
- (56) Mani, R.; Cady, S. D.; Tang, M.; Waring, A. J.; Lehrer, R. I.; Hong, M. *Proc. Natl. Acad. Sci. U.S.A.* **2006**, *103*, 16242.
- (57) Wang, T.; Yao, H.; Hong, M. *J. Biomol. NMR* **2013**, *56*, 139.
- (58) Donald, J. E.; Zhang, Y.; Fiorin, G.; Carnevale, V.; Slochower, D. R.; Gai, F.; Klein, M. L.; DeGrado, W. F. *Proc. Natl. Acad. Sci. U.S.A.* **2011**, *108*, 3958.
- (59) Shen, Y.; Delaglio, F.; Cornilescu, G.; Bax, A. *J. Biomol. NMR* **2009**, *44*, 213.
- (60) Huster, D.; Yao, X.; Hong, M. *J. Am. Chem. Soc.* **2002**, *124*, 874.
- (61) Cady, S. D.; Goodman, C.; Tatko, C.; DeGrado, W. F.; Hong, M. *J. Am. Chem. Soc.* **2007**, *129*, 5719.
- (62) Hong, M.; Doherty, T. *Chem. Phys. Lett.* **2006**, *432*, 296.
- (63) Drechsler, A.; Anderluh, G.; Norton, R. S.; Separovic, F. *Biochim. Biophys. Acta* **2010**, *1798*, 244.
- (64) Traikia, M.; Warschawski, D. E.; Recouvreur, M.; Cartaud, J.; Devaux, P. F. *Eur. Biophys. J.* **2000**, *29*, 184.
- (65) Gawrisch, K.; Parsegian, V. A.; Hajduk, D. A.; Tate, M. W.; Graner, S. M.; Fuller, N. L.; Rand, R. P. *Biochemistry* **1992**, *31*, 2856.
- (66) Rand, R. P.; Fuller, N. L. *Biophys. J.* **1994**, *66*, 2127.
- (67) Thayer, A. M.; Kohler, S. J. *Biochemistry* **1981**, *20*, 6831.
- (68) Tenchov, B. G.; MacDonald, R. C.; Lentz, B. R. *Biophys. J.* **2013**, *104*, 1029.
- (69) Schmidt, N.; Mishra, A.; Lai, G. H.; Wong, G. C. *FEBS Lett.* **2010**, *584*, 1806.
- (70) Mishra, A.; Gordon, V. D.; Yang, L.; Coridan, R.; Wong, G. C. L. *Angew. Chem., Int. Ed.* **2008**, *47*, 2986.
- (71) Kučerka, N.; Nieh, M. P.; Katsaras, J. *Biochim. Biophys. Acta* **2011**, *1808*, 2761.
- (72) Kučerka, N.; Tristram-Nagle, S.; Nagle, J. F. *J. Membr. Biol.* **2005**, *208*, 193.
- (73) Chernomordik, L. V.; Kozlov, M. M. *Annu. Rev. Biochem.* **2003**, *72*, 175.
- (74) Markvoort, A. J.; Marrink, S. J. *Curr. Top. Membr.* **2011**, *68*, 259.
- (75) Chernomordik, L. V.; Leikina, E.; Frolov, V.; Bronk, P.; Zimmerberg, J. *J. Cell Biol.* **1997**, *136*, 81.
- (76) Chen, J.; Lee, K. H.; Steinhauer, D. A.; Stevens, D. J.; Skehel, J. J.; Wiley, D. C. *Cell* **1998**, *95*, 409.
- (77) Weis, W. I.; Brunger, A. T.; Skehel, J. J.; Wiley, D. C. *J. Mol. Biol.* **1990**, *212*, 737.
- (78) Smith, E. C.; Gregory, S. M.; Tamm, L. K.; Creamer, T. P.; Dutch, R. E. *J. Biol. Chem.* **2012**, *287*, 30035.

- (79) Epand, R. M.; Epand, R. F. *Biochem. Biophys. Res. Commun.* **1994**, 202, 1420.
- (80) Epand, R. M.; Epand, R. F.; Martin, I.; Ruyschaert, J. M. *Biochemistry* **2001**, 40, 8800.
- (81) Gabrys, C. M.; Yang, R.; Wasniewski, C. M.; Yang, J.; Canlas, C. G.; Qiang, W.; Sun, Y.; Weliky, D. P. *Biochim. Biophys. Acta* **2010**, 1798, 194.
- (82) Pereira, F. B.; Valpuesta, J. M.; Basañez, G.; Goñi, F. M.; Nieva, J. L. *Chem. Phys. Lipids* **1999**, 103, 11.
- (83) Tristram-Nagle, S.; Chan, R.; Kooijman, E.; Uppamoothikkal, P.; Qiang, W.; Weliky, D. P.; Nagle, J. F. *J. Mol. Biol.* **2010**, 402, 139.
- (84) Kaasgaard, T.; Drummond, C. J. *Phys. Chem. Chem. Phys.* **2006**, 8, 4957.
- (85) Kulkarni, C. V.; Wachter, W.; Iglesias-Salto, G.; Engelskirchen, S.; Ahualli, S. *Phys. Chem. Chem. Phys.* **2011**, 13, 3004.
- (86) Zhang, H.; Neal, S.; Wishart, D. S. *J. Biomol. NMR* **2003**, 25, 173.